Received: 2 May 2022 | Revised: 6 October 2022 | Accepted: 15 October 2022 | Published on: 2 November 2022

DOI: 10.1002/mrm.29516

RESEARCH ARTICLE

Magnetic Resonance in Medicine

On the water–fat in-phase assumption for quantitative susceptibility mapping

Christof Boehm[1] | **Sarah Schlaeger**[2] | **Jakob Meineke**[3] | **Kilian Weiss**[4] | **Marcus R. Makowski**[1] | **Dimitrios C. Karampinos**[1]

[1]Department of Diagnostic and Interventional Radiology, School of Medicine, Klinikum rechts der Isar, Technical University of Munich, Munich, Germany

[2]Department of Diagnostic and Interventional Neuroradiology, School of Medicine, Klinikum rechts der Isar, Technical University of Munich, Munich, Germany

[3]Philips Research, Hamburg, Germany

[4]Philips GmbH Market DACH, Hamburg, Germany

Correspondence
Christof Boehm, Department of Diagnostic and Interventional Radiology, Klinikum rechts der Isar, Ismaninger Str 22, 81675 Munich, Germany.
Email: christof.boehm@tum.de

Funding information
H2020 European Research Council, Grant/Award Number: 677661; Philips Healthcare

Purpose: To (a) define multi-peak fat model-based *effective* in-phase echo times for quantitative susceptibility mapping (QSM) in water–fat regions, (b) analyze the relationship between fat fraction, field map quantification bias and susceptibility bias, and (c) evaluate the susceptibility mapping performance of the proposed *effective* in-phase echoes in comparison to single-peak in-phase echoes and water–fat separation for regions where both water and fat are present.

Methods: *Effective* multipeak in-phase echo times for a bone marrow and a liver fat spectral model were derived from a single voxel simulation. A Monte Carlo simulation was performed to assess the field map estimation error as a function of fat fraction for the different in-phase echoes. Additionally, a phantom scan and in vivo scans in the liver, spine, and breast were performed and evaluated with respect to quantification accuracy.

Results: The use of single-peak in-phase echoes can introduce a worst-case susceptibility bias of 0.43 ppm. The use of *effective* multipeak in-phase echoes shows a similar quantitative performance in the numerical simulation, the phantom and in all in vivo anatomies when compared to water–fat separation-based QSM.

Conclusion: QSM based on the proposed *effective* multipeak in-phase echoes can alleviate the quantification bias present in QSM based on single-peak in-phase echoes. When compared to water–fat separation-based QSM the proposed *effective* in-phase echo times achieve a similar quantitative performance while drastically reducing the computational expense for field map estimation.

KEYWORDS
field map, in phase, quantitative susceptibility mapping, susceptibility

1 | INTRODUCTION

Quantitative susceptibility mapping (QSM)[1] has been applied in tissues outside the brain, for example, to distinguish osteolytic/osteoblastic bone changes in the spine,[2] to characterize lesions and calcifications in breast disease,[1,3] to measure bone density,[4-7] or liver iron overload.[8-10] However, QSM in the body remains challenging for several reasons including the large susceptibility difference between bone, soft tissue, and air and the presence of fat. To obtain a field map without fat phase contributions, multi-echo acquisitions and subsequent extraction of the water–fat model parameters such as the water- and fat-images, R_2^*- and field map[11] are commonly performed. However, water–fat separation-based field-mapping itself is a large field of research and subject to a variety of restrictions and limitations.

First, the echo times have to be carefully selected for a robust separation of water and fat and consequently for the correct estimation of the field map parameter.[12,13] At 3T, optimal echo time step for a 6 echo acquisition has been estimated by Cramer–Rao analysis to be of the order of 1ms.[13] However, such a short echo time step either limits the achievable resolution or the echoes cannot be recorded in a single repetition time (TR), especially while using monopolar gradients. A possible solution to the trade off between echo time selection and resolution is a time interleaved sequence[14] and has successfully been applied to QSM in water–fat regions.[2,5,11] However, such an acquisition comes at the cost of an increased scan time since the echo times are not acquired in a single TR. Therefore, typically a low number of echoes is used resulting in a comparably short maximum echo time. Longer maximum echo times can be desirable for QSM due to the increased phase weighting and the associated increase in sensitivity for the field map parameter.

Second, the separation of water–fat images and the field map is challenging due to the nonconvex inverse problem, where the solution space is known to include several local and global minima.[15,16] A plethora of field-mapping methods have been proposed to solve the field map estimation problem and many of them rely on a spatial smoothness constraint on the field map.[17-19] Graph-cut-based field-mapping methods have been particularly successful in solving the constraint optimization problem. However, graph-cut-based methods are notoriously computationally intensive and can show processing times of up to hours for scans with either a high resolution or a large field of view.[11]

To sidetrack the above problems of water–fat separation-based field-mapping in body regions, gradient echo imaging using only in-phase echoes has been proposed for the estimation of susceptibility and has primarily been used in the spine.[6,7] By definition, in-phase echoes are acquired when water and fat are in phase. Conventionally, a single-peak fat model is assumed for the definition of in-phase echo times. When using in-phase echo times, the signal model is convex within the period of the phasor and thus the field map can robustly be estimated using gradient descent-based nonlinear least squares techniques. However, physiological fat spectra are known to be spectrally complex rendering the definition of single-peak in-phase echo times problematic.[20] The use of single-peak in-phase echo times has been shown to introduce significant susceptibility quantification bias[21] in regions where the fat spectrum is spectrally complex.

Therefore, the purpose of this work is to (a) generalize the approach of single-peak in-phase echoes to the use of *effective* multipeak in-phase echo times, (b) to investigate the correlation between fat fraction, field map estimation bias and susceptibility bias and to (c) demonstrate the feasibility of *effective* multipeak in-phase echo times to successfully alleviate the quantification bias of single-peak in-phase echoes. Therefore, susceptibility mapping based on *effective* multipeak in-phase echoes, conventional single-peak in-phase echoes and water–fat separation were compared in a numerical liver simulation, a phantom and in vivo in the liver, the spine, and the breast.

2 | METHODS

Multipeak effective in-phase echo times

In regions where water and fat are present, the well-established single-R_2^* multipeak water–fat signal model can be used to describe the voxel signal evolution with time as follows:[22]

$$\begin{aligned} \boldsymbol{s}(t_n) &= (\rho_W + c_n \rho_F)\, e^{\gamma t_n}, \quad \gamma = i2\pi f_B - R_2^*, \\ c_n &= \sum_{p=1}^{P} a_p e^{i2\pi \Delta f_p t_n}, \quad \text{with} \quad \sum_{p=1}^{P} a_p = 1, \end{aligned} \tag{1}$$

where t_n are the echo time points, ρ_W and ρ_F are the complex signal of the water and fat components with an equal transverse relaxation rate R_2^* and f_B is the field map. The fat spectrum is assumed to have P spectral peaks with corresponding relative amplitudes a_p and chemical shift Δf_p. Conventionally, for the definition of in-phase echo times, the fat spectrum is assumed to have only one spectral peak $P = 1$. Thus, Equation (1) can be simplified to

$$\boldsymbol{s}(t_n) = \left(\rho_W + \rho_F e^{i2\pi f_p t_n}\right) e^{\gamma t_n}, \quad \gamma = i2\pi f_B - R_2^*, \tag{2}$$

where f_p is the chemical shift of a single fat peak. Under the above assumption of only one spectral peak, the water and fat signal are in-phase when the following condition $e^{i2\pi f_p t_n} = 1 \Leftrightarrow f_p \cdot t_n = b, b \in \mathbf{N}$ for the fat-phasor is met. Often, the methylene peak is set as f_p[23] due to its predominant amplitude in different fat compositions and has a chemical shift of −3.4 ppm relative to water[24] and is presently employed.

In case of the more accurate multipeak signal model in Equation (1), the definition of in-phase echo times is not possible due to the complexity of the fat-phasor where at any time after $t = 0$ the different fat constituents are never simultaneously aligned again. However, *effective* in-phase echoes can be defined, meaning the time points, where the fat-phasor in Equation (1) meets the condition $\angle c_n = 0$, representing the time points where the phase of the fat-phasor is zero.

2.1 | Field map estimation

For the field map estimation from complex multi-echo data a graph-cut algorithm was used.[11] In the case of water–fat separation based field map estimation, the graph-cut method was used as described in Reference 11. In the case of single-peak and multipeak in-phase echoes, the signal model in the graph-cut was reduced to a single species estimation. Specifically, the term describing the contributions of fat was removed since both the single-peak and the multipeak in-phase echoes are hypothesized to contain no phase contributions of fat.

2.2 | Numerical simulations

2.2.1 | Single voxel simulation

For the estimation and visualization of the difference between conventional single-peak and *effective* multipeak fat-model and to find the *effective* multipeak echo times, a single voxel simulation was performed using Equation (1) with either a single-peak fat spectral model using the above chemical shift frequency, a fat-model specific to bone marrow[25] or fat spectral model specific to the liver,[26] a fat fraction of 70%, $R_2^* = 30$ (Hz) and $f_B = 0$. The bone marrow and the liver spectral fat model both have nine fat peaks. The position of the fat peaks is $\Delta f = [-3.8, -3.4, -3.1, -2.68, -2.46, -1.95, -0.5, 0.49, 0.59]$ ppm for both models. The relative amplitude of the fat peak is $a = [0.09, 0.583, 0.06, 0.085, 0.06, 0.015, 0.04, 0.01, 0.057]$ ppm for the bone marrow model and $a = [0.088, 0.642, 0.058, 0.062, 0.058, 0.006, 0.039, 0.01, 0.037]$ ppm for the liver model, respectively. The two spectral models were selected based on the evidence that liver and adipose tissue have different triglyceride composition. The fat fraction and R_2^* were selected for a realistic and clear visualization of the signal evaluation. The variation of both parameters do not influence the zero crossings of the fat phasor.

2.2.2 | Monte Carlo simulation

A Monte Carlo simulation was performed for assessing the field map estimation error at different fat fractions using both conventional single-peak or *effective* multipeak in-phase echo times. The fat fraction values were varied from 0% to 100%, $R_2^* = 30$(Hz) and $f_B = 0$ were used. Independent Gaussian noise was added to the real and imaginary part of the echo data with an signal-to-noise ratio (SNR) of 100. The SNR was defined as the maximum signal amplitude of the first echo divided by the SD of noise. Based on the above values, the signal at different time points was simulated using Equation (1) with the single-peak fat model, the multipeak fat liver model or the multipeak bone marrow fat model. Subsequently, the field map from the three different signals were estimated for each fat fraction using each, the single-peak in-phase echoes and the *effective* multipeak in-phase echoes based on the liver and bone fat-model. Based on the above simulation, the accuracy of field map estimation choosing the echo times in accordance to the underlying fat model as well as cross-model correlation were estimated.

2.2.3 | Correlation between field map estimation error and susceptibility quantification bias

In order to quantify how the field map estimation error translates into susceptibility error without the potential bias of a selected inversion method, a simulation of a sphere with varying susceptibility difference from outside to inside and of an infinite flat surface of two materials with a susceptibility difference was performed. The susceptibility map was forward simulated to a field map and the field map difference was measured at the surface.

2.2.4 | Numerical liver simulation

In order to assess the quantification bias induced by the in-phase assumption in a realistic anatomy, a numerical

simulation based on the Duke phantom was performed using the annotated geometrical data from Reference 27. Each tissue was assigned with either their literature value or values extracted from in vivo scans and forward simulated using Equation (1). To account for the significantly different fat-models of the liver and other fatty tissues, the above liver fat-model was used within the liver and in all other fatty tissues the bone marrow model was used. In the simulation, either conventional water–fat separation echo times with six echoes, $TE_{min}/\Delta TE = 1.0$ ms, conventional single-peak in-phase echo times or *effective* in-phase echo times for the two above-mentioned fat-models were used. In the case of in-phase echo times the first three echo times were used due to there equidistant nature (see below in Results). A background field was simulated based on air outside the subject (9.94 ppm[28]) and in the lungs (13.36 ppm[29]). An SNR of 50 was added similar to the above Monte Carlo simulation. The field map, water(–fat)-images and R_2^*-map were estimated using a graph-cut algorithm.[11] The field maps were inverted to a susceptibility map using a linear total field inversion algorithm.[30] Since the linear total field inversion algorithm method only obtains relative susceptibility maps, the susceptibility maps were referenced using the subcutaneous fat layer. Within the subcutaneous fat layer the susceptibility distribution is assumed to mainly originate from fatty tissue and not altered by diseases such as hepatic iron overload.[8] Normalized root mean square errors (NRMSE) were calculated in reference to the ground truth.

2.2.5 | Phantom measurements

To validate the numerical results, a scan of a vial filled with peanut oil in the center of a water reservoir was performed. Scanning was performed on a 3 T scanner (Ingenia Elition, Philips Healthcare) using a monopolar time-interleaved multi-echo gradient echo sequence[14] for reference water–fat separation, acquiring six echoes with 3 echoes per interleave. An isotropic voxel size of 1.5 mm, a field of view =[120,120, 141], $TE_1 = 1.23$ ms and $\Delta TE = 0.99$ms were used. For the *effective* in-phase echo times a fat model specific to peanut oil was used.[31] Both the single peak in-phase echo times and the *effective* in-phase echo times were temperature corrected[32] to 23°C and were recorded with $TE_{\text{single peak}} = [2.21, 4.42, 6.63]$ ms and $TE_{\text{peanut oil}} = [2.29, 4.44, 6.59]$ ms, respectively. The above processing of graph-cut-based field-mapping and linear total field inversion algorithm dipole inversion was used and the difference susceptibility between an region-of-interest (ROI) in the vial and the water reservoir was measured.

2.3 | In vivo measurements

The aforementioned processing of graph-cut-based field-mapping followed by linear total field inversion algorithm QSM was applied in in vivo scans of the spine, the breast and the liver of 10 volunteers, where in six volunteers only the spine was acquired, in three volunteers the spine and liver were acquired and in one subject only the breast was acquired. Approval by the institutional review board (Klinikum rechts der Isar, Technical University of Munich) was granted for the scans and informed consent was received by all subjects. Scanning was performed on the aforementioned scanner. Reference field maps were estimated using the above monopolar time-interleaved multi-echo gradient echo sequence, where the liver fat model was used for the liver scan and the bone marrow model for the scan of the spine and breast, respectively. In all anatomies scans based on conventional single-peak in-phase echoes were performed. Additionally, the liver was scanned once with *effective* multi-peak echo times based on the liver model and once based on the bone marrow model. The spine and breast were scanned once with *effective* multipeak in-phase echo times based on the bone marrow model. The scanning parameters for each anatomy are given in Table 1. For a quantitative assessment of the results, a difference measurement within the susceptibility map was performed between different tissue types. Fat[8] and paraspinal muscles[33] have previously been used for referencing of susceptibility maps and hence were presently adopted. For the liver scan, the difference between subcutaneous fat and a ROI in the liver of the size of $\sim 12\,cm^3$ and an ROI in the paraspinal muscle of the size of $\sim 4\,cm^3$ and the ROI in the liver were measured (see Figure 5). For the subcutaneous fat layer mask, all voxels with a fat fraction greater than 75% were selected. In the lumbar spine scans, the difference between the posterior subcutaneous fat layer (orange arrow in Figure 6) and the spinal canal between the upper plate of the L3 vertebra and the base plate of the L5 vertebra was measured. Since in healthy adults the spinal cord ends at the height of the L1/L2 vertebrae, the segmented part of the spinal canal is predominantly filled with cerebrospinal fluid (CSF, white arrow) which is often used in brain QSM for referencing.[34] The subcutaneous fat layer mask was generated as for the liver scan. The CSF region was manually segmented. In the breast scan, the difference between fatty and fibroglandular tissue in the right breast was measured. First, the right breast was segmented using the deep neural network and weights from Reference 35. Within the right breast, the fat mask was again based on all voxels with a fat fractions greater than 75%. The fibroglandular tissue mask was based on all voxels with a fat fraction from 0%–20%.

TABLE 1 MR scan parameters for the in vivo acquisitions for the respective anatomy

Parameter	Liver	Spine	Breast
Field of view	$400 \times 320 \times 180$ mm^3	$220 \times 220 \times 79.2$ mm^3	$220 \times 382 \times 192.4$ mm^3
Voxel size	$2 \times 2 \times 5$ mm^3	1.8 mm isotropic	1.3 mm isotropic
Flip angle	3°	3°	3°
Acceleration	Compressed sensing ($R = 4$)	None	Compressed sensing ($R = 6$)
Acquisition for water–fat separation			
Type	Interleaved (2)	Interleaved (2)	Interleaved (2)
TE	$N_{TE} = 4$ $TE_{min} = 1.09$ ms $\Delta TE = 0.80$ ms	$N_{TE} = 6$ $TE_{min} = 1.33$ ms $\Delta TE = 1.05$ ms	$N_{TE} = 6$ $TE_{min} = 1.58$ ms $\Delta TE = 1.28$ ms
TR	4.7 ms	8.1 ms	10 ms
Scan time	0:16 min	3:12 min	4:15 min
Acquisition of *effective*multipeak in-phase echoes			
Type	Single acquisition (all echoes in one TR)	Single acquisition (all echoes in one TR)	Interleaved (2)
TE	(Liver model) $N_{TE} = 3$ $TE_{min} = 2.35$ ms $\Delta TE = 2.24$ ms	(Bone marrow model) $N_{TE} = 3$ $TE_{min} = 2.38$ ms $\Delta TE = 2.22$ ms	(Bone marrow model) $N_{TE} = 4$ (3 used) $TE_{min} = 2.38$ ms $\Delta TE = 2.22$ ms
TR	8.5 ms	8.3 ms	11 ms
Scan time	0:17 min	1:52 min	3:21 min

Note: All acquisitions used monopolar gradients.

On the fibroglandular tissue mask, binary erosion was applied once in order to remove the skin layer from the mask. All manual segmentations namely, the drawing of the ROI in the subcutaneous fat, the ROI in the liver, the ROI in the paraspinal muscle and the spinal chanel between L3 and L5 were performed by a radiologist (with 6 years experience).

3 | RESULTS

3.1 | Numerical simulations

3.1.1 | Single voxel simulation

Figure 1 shows the signal evolution of a voxel containing both water and fat for different fat models. The dashed lines in gray indicate the time points where water and fat are in-phase in the case of the single-peak assumption ($TE_{min}/\Delta TE = 2.3$ ms). The dashed lines in green indicate the time points, where the phase is zero and refer to the *effective* in-phase echo times The first six *effective* in-phase echoes are $TE = [2.38, 4.6, 6.81, 9.17, 11.62, 13.92]$ and $TE = [2.35, 4.59, 6.83, 9.2, 11.6, 13.89]$ for the bone marrow and the liver model, respectively. In the case of the bone marrow model the first three echoes are almost equidistant. Echo times of $TE = [2.38, 4.6, 6.82]$ ($TE_{min}/\Delta TE = 2.38/2.22$ ms) were subsequently used as the *effective* in-phase echo times for the bone marrow fat model. In the case of the liver model the first three echo times are exactly equidistant with $TE_{min}/\Delta TE = 2.35/2.24$ ms and are subsequently referred to as *effective* in-phase echo times for the liver fat model.

3.1.2 | Monte Carlo simulation

Figure 2 shows the quantification bias of the field map as a function of the fat fraction for different fat models. The plots in the first column show the quantification bias of the single-peak in-phase assumption. For the single-peak assumption and a voxel with a fat fraction of 100% the field map error is almost −0.1 ppm for the liver fat model and −0.13 ppm for the bone marrow fat model, respectively (yellow background). The plots on the diagonal (blue background) reveal that the use of *effective* multi-peak in-phase echoes can reduce the field map quantification bias down to the noise level for both multipeak fat models. Measuring with *effective* in-phase echo times cross model (green background), the field map quantification bias for voxel with a fat fraction of 100% is significantly smaller than

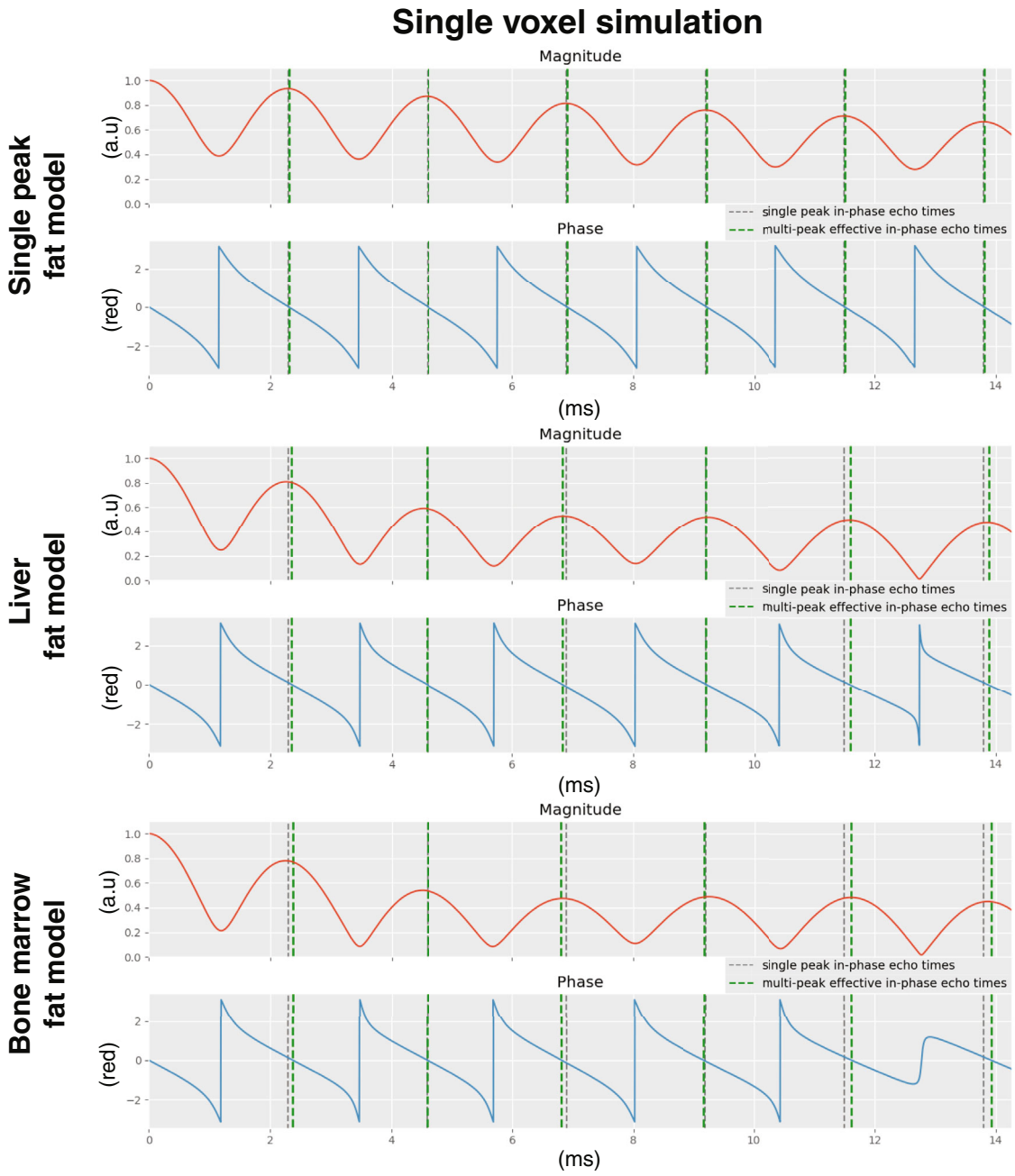

FIGURE 1 Magnitude and phase evolution for different fat models in a voxel containing both water and fat. The dashed line in gray refer to the time points at which the phase of fat in the single-peak assumption is zero ($TE_{min}/\Delta TE = 2.3$ ms). The dashed lines in green refer to the time points, where the fat phase is generally zero. For the single-peak fat model both time points coincide. In case of both the multi-peak liver and the bone marrow model the green and gray lines generally do not coincide and are shifted in both directions around the single-peak in-phase time points. Most importantly, in both multipeak fat models the time points where the fat phasor is zero are not equidistant and read TE = [2.38, 4.6, 6.81, 9.17, 11.62, 13.92] and TE = [2.35, 4.59, 6.83, 9.2, 11.6, 13.89] for the bone marrow and the liver fat spectrum model, respectively. While the first three echo times for liver model are equidistant this is not true for the bone marrow fat model. However, in the case of the bone marrow model either the first or the third echo time can be shifted by 0.01 ms to obtain three equidistant echoes

for the single-peak assumption and is 0.03 ppm. The plots with the red background show the correlation for the case of fatty tissue with only a single-fat peak estimated with *effective* multipeak in-phase echo times. Fatty tissue with only a single-fat peak is nonphysiological and is given for completeness. Noteworthy is that the correlation for physiological meaningful combinations (second and third row) are nonlinear. The correlations are well approximated using a second-order polynomial (see χ^2-test in each subplot's legend).

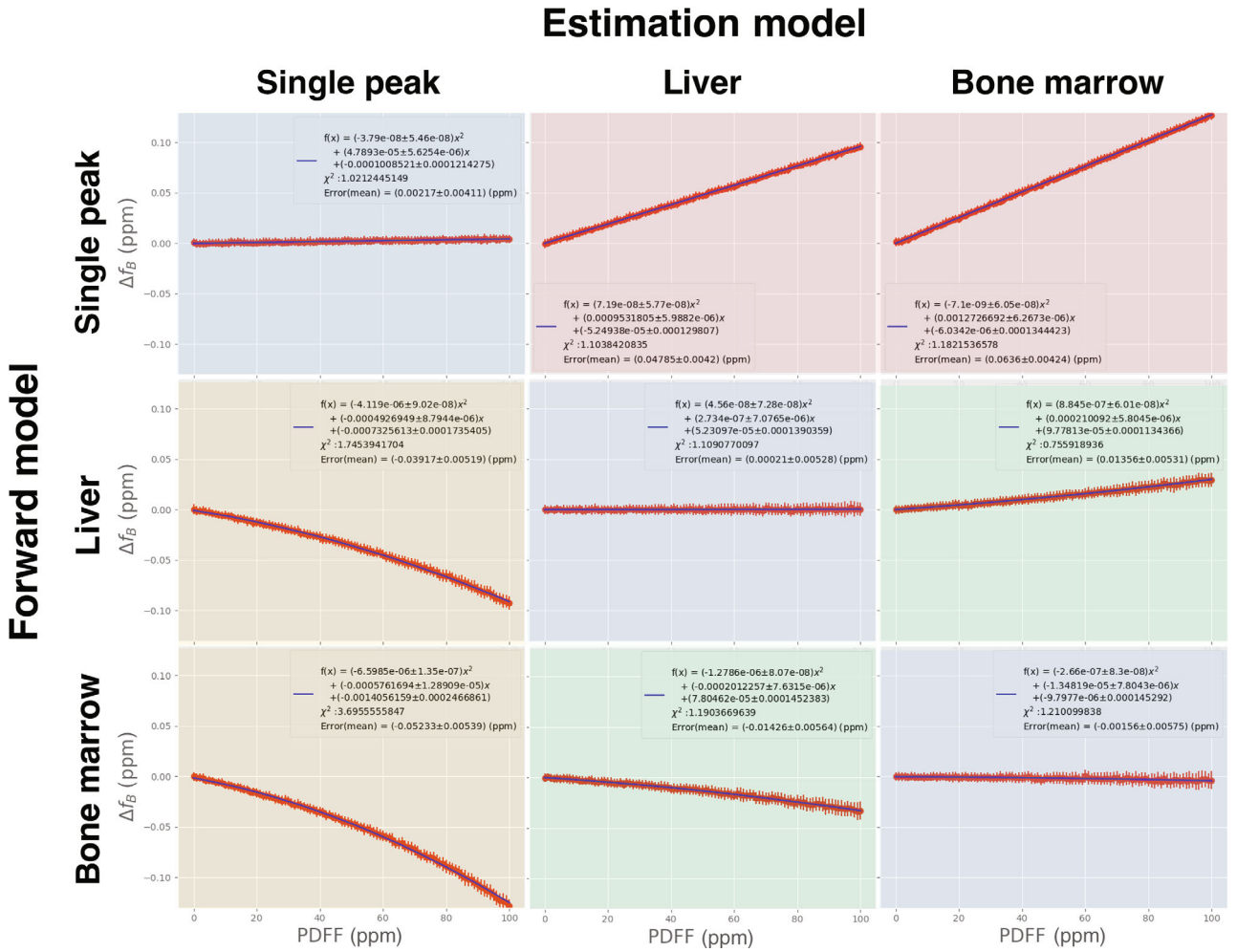

FIGURE 2 Analysis of the quantification bias of the field map in dependence of the fat fraction for different in-phase models. Each row shows the bias for the different fat model which were used to forward simulate the signal, while each column shows the bias for the different fat models which were used to define the (*effective multi-peak*) in-phase echo times used for the field map estimation. On the diagonal (blue background) plots, the results are shown when for a fat model the corresponding (*effective*) in-phase echo times were used. Using the correct in-phase echoes, the field map quantification bias can be alleviated for each fat model. When single-peak in-phase echo times are used to measure in the liver or the bone marrow (yellow background). The field map quantification bias correlates quadratically with fat fractions and reaches up to −0.1 ppm for the liver model and −0.13 ppm for the bone marrow model, respectively. Measuring with *effective* in-phase echo times cross model (green background), the field map quantification bias also correlates quadratically with fat fraction. In a voxel with a fat fraction of 100% the field map quantification bias in a cross-model measurement is significantly smaller than for the single-peak assumption and is 0.03 ppm. The case where the voxel only contains a single species, but are estimated with a multipeak fat model (red background) is only given for completeness.

3.1.3 | Correlation between field map estimation error and susceptibility quantification bias

Figure S1 shows how the field map quantification error propagates into susceptibility mapping error without the bias of the selected dipole inversion method. The field map quantification error correlation for a spherical surface and an infinite surface is −0.304 and −0.332 when the surface is parallel to B_0 and 0.608 and 0.664 when the surface is perpendicular to B_0, respectively. The difference between both surface types is 9.2%. The field map error in a voxel with a fat fraction of 100% measured with single-peak in-phase echoes hence translates into worst-case susceptibility estimation error of $\frac{-0.1\text{ppm}}{-0.304} = 0.33$ ppm in the liver and $\frac{-0.13\text{ppm}}{-0.304} = 0.43$ ppm in bone marrow, respectively.

3.1.4 | Numerical liver simulation

Figure 3 shows field- and susceptibility-mapping results in a numerical liver simulation. The second row shows the reference field map and the difference between reference

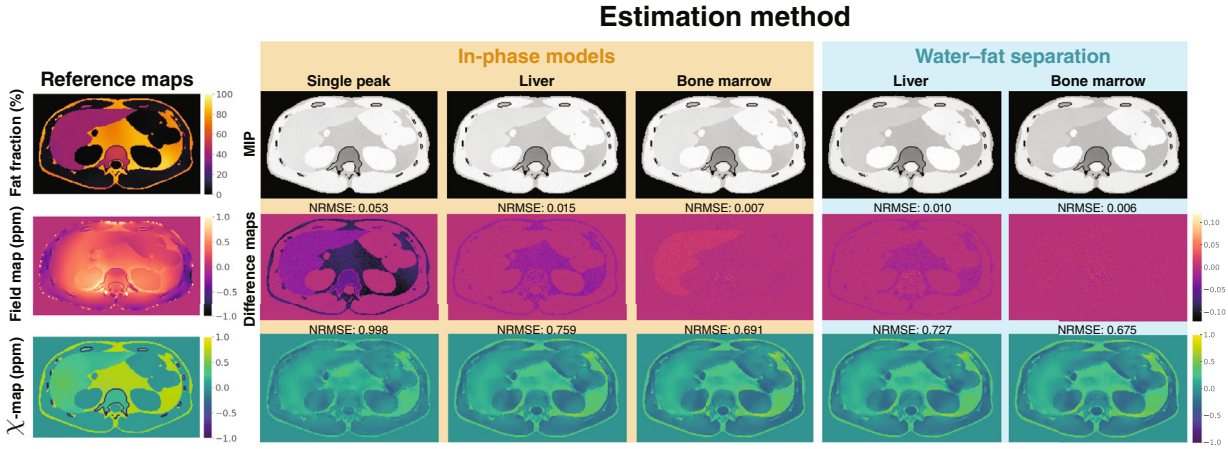

FIGURE 3 Results of field- and susceptibility-mapping in a numerical liver simulation. The first column shows the reference fat fraction, field map and susceptibility map used in the forward simulation. The rest of columns show the maximum intensity projection across echo times, the difference field maps with respect to the reference map and the susceptibility maps. The in-phase models (yellow background) refer to an acquisition based on the respective echo times specific to the fat model. For the water–fat separation-based estimation (blue background), the same echo times were used while in the separation the respective fat models were employed. The field map quantification bias correlates (i) with the fat fraction and (ii) with the employed estimation method. The use of single-peak in-phase echoes shows the largest field- and susceptibility-mapping error. Results based on *effective* bone marrow in-phase echoes (i) perform better than the liver model echo times and (ii) the normalized root mean square errors is comparable to water–fat separation-based results. However, general underestimation of susceptibility in all methods can be observed.

field map and estimated field map for each method. The difference map for the single-peak in-phase assumption yields the largest NRMSE of 0.053 ppm. The offset is dependent on the fat fraction and is always negative. The field map difference map of the liver *effective* in-phase model yields a NRMSE of 0.015 ppm. Using *effective* in-phase echoes based on the liver fat model, no field map quantification bias can be observed within the liver. However, a negative correlation with the fat fraction in other fatty tissue can be observed which is significantly smaller than in the single-peak in-phase echo-based map. The field map difference map based on the bone marrow model has an NRMSE of 0.007 ppm and quantification bias only within the liver. The quantification bias in the case of the bone marrow model has a positive correlation with the fat fraction. The correlations observed in the numerical liver simulation are in good agreement with the cross-model correlations shown in Figure 2. The error of the referenced susceptibility maps directly correlates with the error of the underlying field map. The higher the field map error, the higher the susceptibility error. However, a general overestimation of susceptibility values can be observed even in the method with the lowest NRMSE.

3.1.5 | Phantom measurements

In the phantom scan shown in Figure 4 the difference between the ROI in the vial and the water reservoir yielded −0.068 ppm for single-peak in-phase echoes, 0.035 for *effective* in-phase echoes and −0.039 for water–fat separation-based susceptibility mapping. The use of conventional single-peak in-phase echo times shows a underestimation of field map and susceptibility values in the vial. Furthermore, in the susceptibility map based on single-peak in-phase echoes strong streaking artifacts around the oil-filled vial can be observed. Field-mapping and QSM results based on *effective* multipeak in-phase echoes show similar results to water–fat separation-based estimation. Mean, SD, and ROI size of the water reservoir and the oil vial can be found in Table S1.

3.2 | In vivo measurements

In a exemplary scan of the liver shown in Figure 5 the used ROIs in the paraspinal muscle and the liver for the difference measurements are depicted. The mean difference across all subject between the subcutaneous fat layer and the ROI in the liver yielded (0.15 ± 0.01) ppm for single-peak in-phase echoes, (0.24 ± 0.06) ppm and (0.28 ± 0.08) ppm for *effective* multipeak in-phase echoes based on the liver and bone marrow fat model, respectively, and (0.29 ± 0.05) ppm based on water–fat separation-based susceptibility mapping. The mean difference across all subject between the ROI in the back muscle and the ROI in the liver yielded (-0.03 ± 0.04) ppm for single-peak in-phase echoes, (-0.08 ± 0.05) ppm and

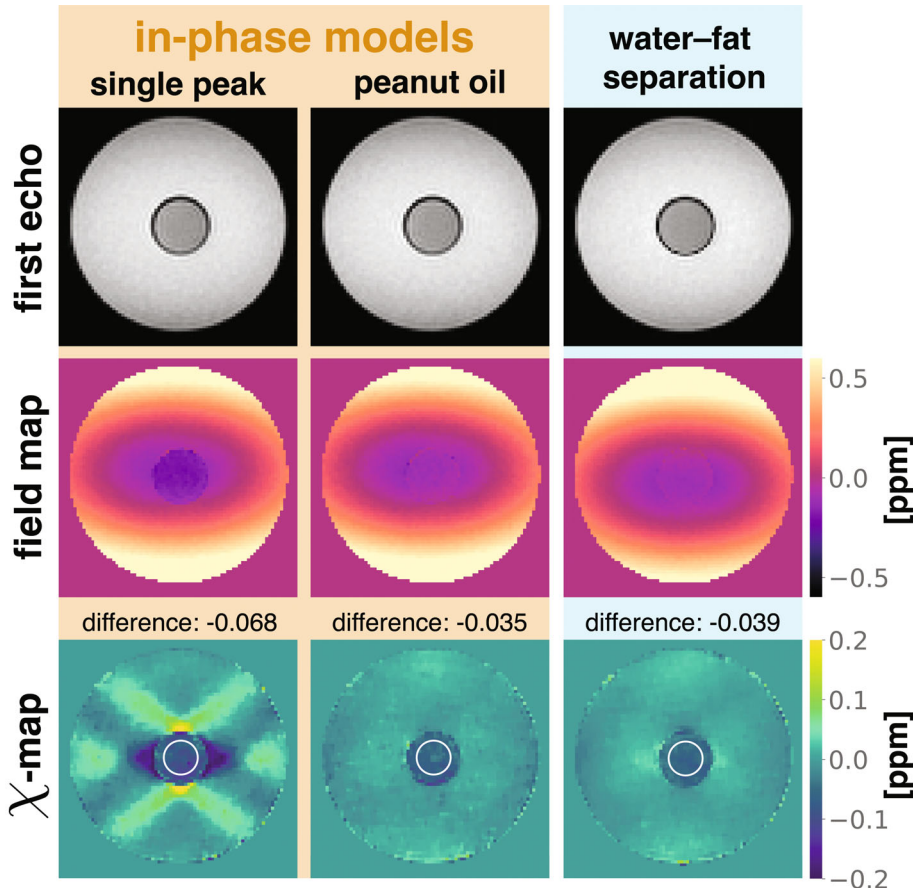

FIGURE 4 First echo (first row), field-mapping (second row) and susceptibility mapping (last row) results in the scan of a oil filled vial in a water reservoir. The in-phase models (yellow background) refer to an acquisition based on the respective echo times specific to the model. Both the in-phase and the water–fat separation fat model used fat spectracs temperature corrected to 23°C. For comparison, the difference susceptibility between an region-of-interest in the vial (white circle) and the water reservoir was measured. The single-peak in-phase estimation shows an underestimation in field map and susceptibility value and strong streaking artifacts around the vial in the susceptibility map. The use of peanut oil model-based *effective* in-phase echoes shows similar results to reference water–fat separation-based estimation. Specifically, the differences measurement between the vial and the water reservoir yield −0.068 ppm for the single-peak in-phase estimation, −0.035 ppm for the *effective* multi-peak in-phase echoes and −0.039 ppm for water–fat separation-based estimation.

(−0.10 ± 0.06) ppm for *effective* multipeak in-phase echoes based on the liver and bone marrow fat model, respectively, and (−0.12 ± 0.09) ppm based on water–fat separation-based susceptibility mapping.

Using *effective* bone marrow in-phase echo times in the spine (exemplary Figure 6), similar susceptibility values in the anterior subcutaneous fat (orange arrows) can be observed as in the susceptibility map based on a water–fat separation-based field map. The use of single-peak in-phase echoes significantly underestimate regions with high fat fractions. Particularly noteworthy is the CSF region in the susceptibility map based on single-peak in phase echoes (white arrow) that shows strong streaking artifacts. The CSF region in the susceptibility map based on water–fat separation and on *effective* multipeak in-phase echoes is less effected by streaking artifacts. Furthermore, the susceptibility map based on water–fat separation shows the highest SNR and hence minimal noise compared to both in-phase maps. The mean susceptibility difference across the nine subjects between the subcutaneous fat layer and the CSF yielded (0.07 ± 0.07) ppm for single-peak in-phase echoes, (0.30 ± 0.09) ppm for *effective* multipeak in-phase echoes based on the bone marrow model and (0.31 ± 0.08) ppm for water–fat separation-based susceptibility mapping, respectively.

The in vivo breast scan shown in Figure 7 yielded comparable results. The water–fat separation-based susceptibility allowed for a good delineation between fatty and dense breast tissue (arrow) and showed the least noisy image. A lot of contrast between the tissue types was lost in the single-peak-based map and noise was increased. The susceptibility map based on *effective* in-phase echo times showed a similar contrast between the tissue types at the arrow position. However, also an increase in residual background field removal artifacts was observed especially in proximity to the sternum and thoracic bones. The susceptibility difference measurement between fatty breast tissue and fibrograndular tissue yielded 0.22 ppm for single-peak in-phase echoes, 0.29 ppm for *effective* multipeak in phase echoes based on the bone marrow model and 0.30 ppm for water–fat separation-based susceptibility mapping, respectively.

The correlation of the difference measurements between reference water–fat separation-based susceptibility estimation and an estimation based on (*effective*) in-phase echoes yields a strong correlation between *effective* in-phase echoes based on the bone marrow fat model.

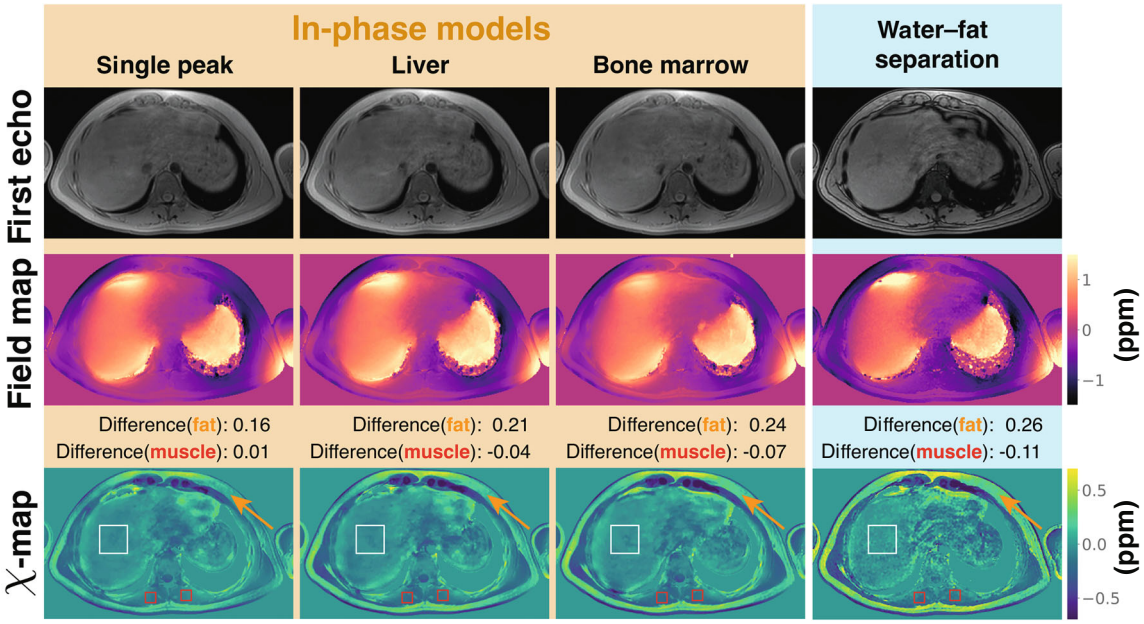

FIGURE 5 First echo (first row), field-mapping (second row) and susceptibility-mapping (last row) results in the liver scan of a volunteer. The in-phase models (yellow background) refer to an acquisition based on the respective echo times specific to the model. The field map quantification bias correlates (i) with the fat fraction and (ii) with the employed estimation method. For comparison of the different susceptibility estimation methods, the difference between the subcutaneous fat layer (orange arrow) and an region-of-interest in the liver (white box) was measured and is given above the susceptibility maps. The susceptibility maps based on single-peak and on *effective* in-phase echoes based on the liver model show a significant underestimation of the difference when compared to water–fat separation-based susceptibility estimation. Susceptibility mapping based on *effective* in-phase echoes based on the bone marrow modal only show a small deviation water–fat separation-based result.

Using single-peak in-phase echoes results in a significant underestimation of susceptibility and an increase in variability (Figure 8). *effective* in-phase echoes based on the liver fat model shows a moderate underestimation of susceptibility values. Mean, SD, and ROI size for each subject, anatomy and ROI can be found in Table S1.

4 | DISCUSSION

The present study aimed to enable the field map estimation and subsequent susceptibility mapping in water–fat regions without the need of the often computational intensive water–fat separation. First, the concept of *effective* multipeak in-phase echo times was introduced which generalizes single fat peak in-phase echo times to the more physiological meaningful multipeak fat models. Specifically, for a in vivo liver, a in vivo bone marrow and a ex vivo peanut oil multipeak fat spectral model the *effective* multipeak in-phase echo times were defined as the time points, where the sum of the individual fat phasors is zero. These time points have the same *effect* in the multipeak water–fat signal model as in-phase echoes in the single-peak model, meaning the nulling of fat phase contributions by echo time selection. The study then quantified the field map estimation error for single-peak in-phase echoes and multipeak *effective* in-phase echoes for the above in vivo multipeak fat models at different fat fractions. Next, the study estimated how field map quantification bias translates into susceptibility map based on a forward simulation at an infinite surface and a sphere. The different echo times were then tested in a numerical simulation of the liver and in vivo measurements in the liver, spine, and breast. In the simulation, multipeak *effective* in-phase echo times based on the bone marrow model was able to achieve a significantly reduced NRMSE when compared to conventional single-peak-based in-phase echo times. In a phantom scan, QSM based on *effective* in-phase echoes yielded the same results as water–fat separation-based estimation while single-peak in-phase echo estimation showed a underestimation of susceptibility of the oil vial and strong streaking artifacts. In vivo, multipeak *effective* in-phase echo times showed comparable results to water–fat separation-based field- and susceptibility-mapping and was able to especially alleviate the quantification bias of the single-peak in-phase echoes-based estimation in regions with high fat fraction such as the subcutaneous fat layer or fatty breast tissue. Furthermore, the study showed that the bone marrow fat model yields improved susceptibility mapping results in the liver when compared to the use of a fat

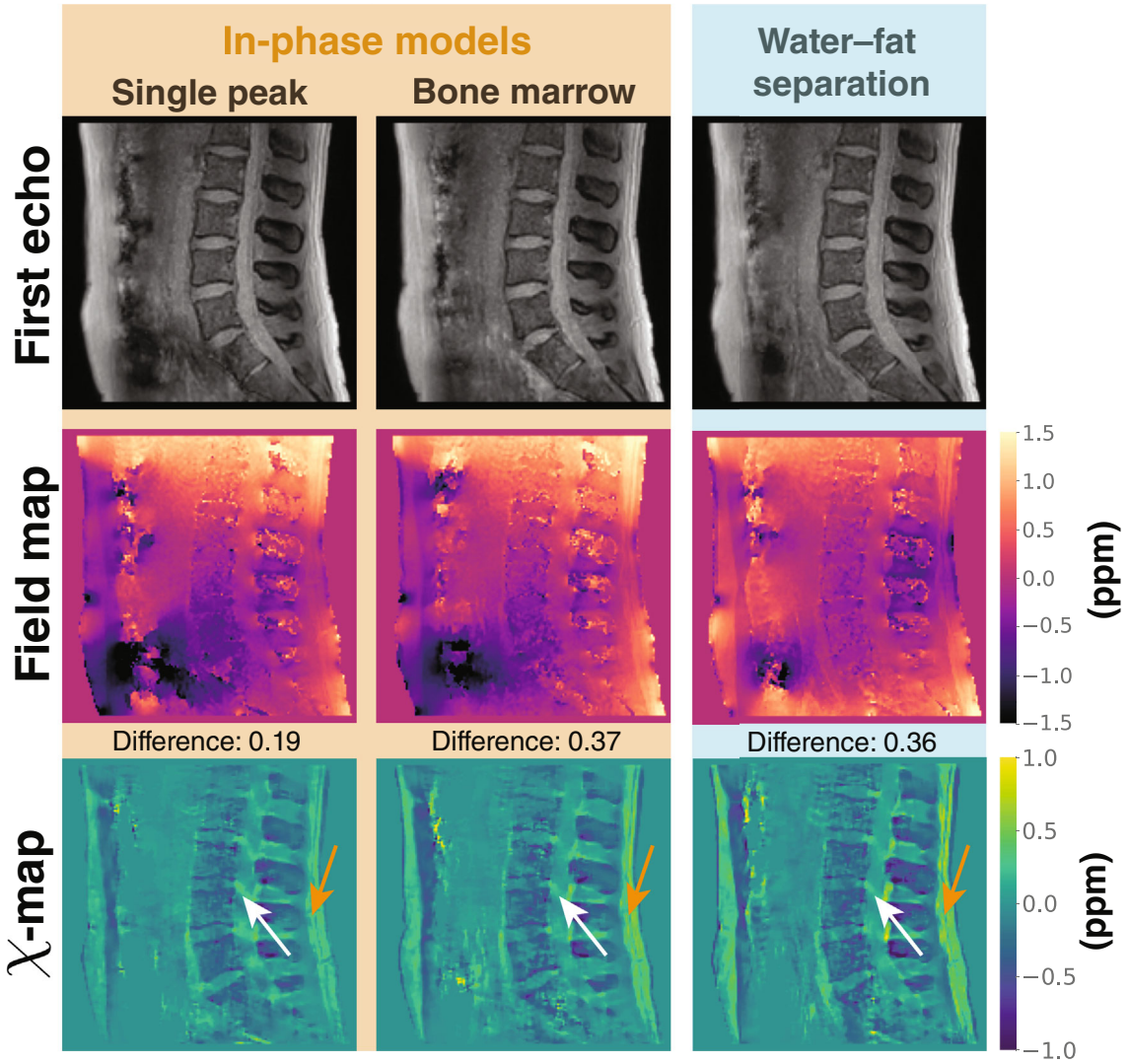

FIGURE 6 First echo (first row), field-mapping (second row) and susceptibility-mapping (last row) results in the scan of the lumbar spine in a volunteer. The in-phase models (yellow background) refer to an acquisition based on the respective echo times specific to the model. For comparison of the different susceptibility estimation methods, the difference between the posterior subcutaneous fat layer (orange arrow) and the cerebrospinal fluid (CSF, white arrow) was measured and is displayed above the susceptibility maps. The susceptibility map based on single-peak in-phase echoes shows a significant underestimation in the subcutaneous fat layer and strong streaking artifacts in the CSF when compared to both *effective* multipeak in phase echo times and water–fat separation-based susceptibility-mapping. The susceptibility map based on the water–fat separation shows the highest signal-to-noise ratio due to the acquisition of twice as many echo time points compared to in-phase acquisition. The differences measurement between the CSF and subcutaneous fat yield 0.38 ppm for the single-peak in-phase estimation, 0.61 ppm for the *effective* multipeak in-phase echoes and 0.68 ppm for water–fat separation-based estimation.

model specific to the liver fat composition. The use of (*effective*) in-phase echoes can be advantageous for several reasons including (a) the simplified signal model, (b) reduced scan time, and (c) the selection of larger echo time steps compared to water–fat separation-based sequences.

First, the simplified signal model allows for the robust estimation of the field map parameter by using least squares techniques followed by an unwrapping step that are both generally computationally inexpensive when compared to water–fat separation-based techniques such as IDEAL[36] or generalized IDEAL-like methods,[37] which iteratively alternate between linear and nonlinear terms, or graph-cut-based methods[11,18,19,38] that are known to yield a high accuracy in field map quantification at the cost of long-run times of several minutes up to hours.[11] Although the presently employed field-mapping technique for the in-phase echoes is based on a graph-cut algorithm introduced in Reference 11, the reduction of computational cost within the graph-cut method is significant in the case of a convex cost function within one period. The underlying graph-cut algorithm

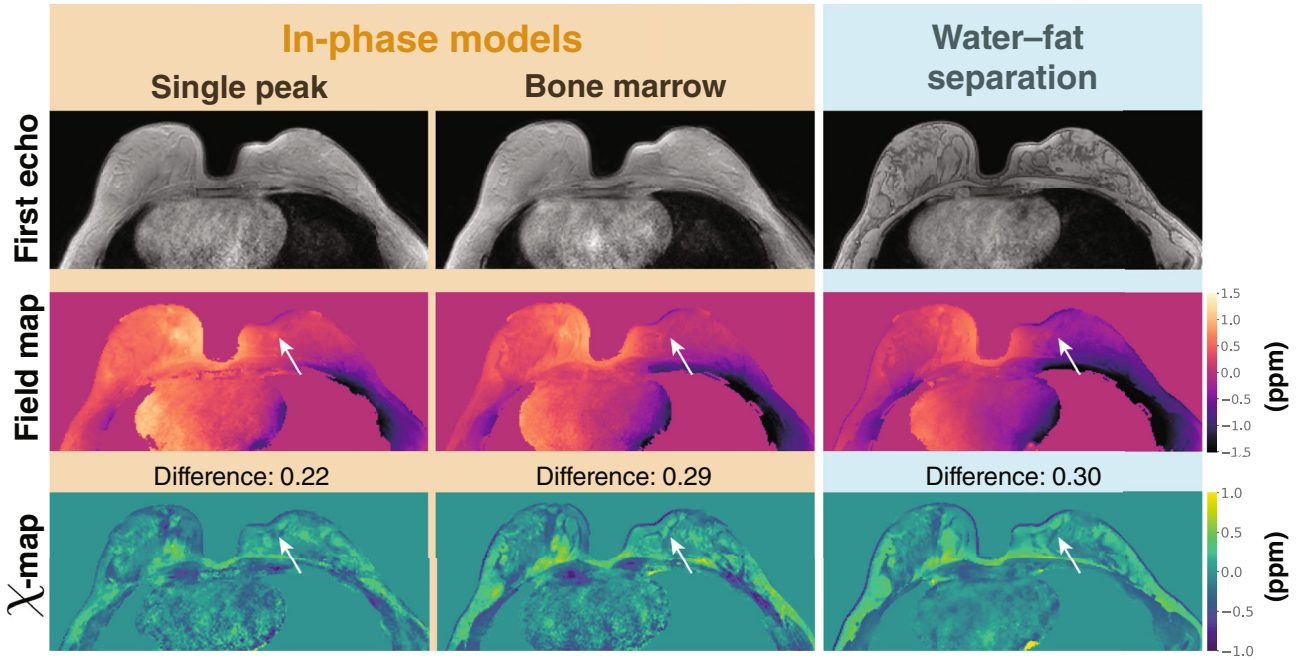

FIGURE 7 First echo (first row), field-mapping (second row) and susceptibility-mapping (last row) results in the scan of the breast in a volunteer. The in-phase models (yellow background) refer to an acquisition based on the respective echo times specific to the model. For comparison of the different susceptibility estimation methods, in the righ breast (white arrow) the difference between fatty and nonfatty breast tissue was measured and is given above the susceptibility maps. The susceptibility map based on in-phase echoes (first column) shows a underestimation of the fatty breast tissue when compared to the water–fat separation-based susceptibility estimation (third column). The results based on *effective* multipeak in-phase echo times (second column) shows a similar difference to the water–fat separation based. However, the bone marrow in-phase susceptibility map shows strong residual susceptibility variations especially between the breast and close to the lungs originating from an improper removal of the background field. Additionally, an increase in noise can be observed in the in-phase-based susceptibility maps.

(boykov-kolmogorov) has a worst case complexity of $\mathcal{O}(n^2 m|C|)$, where n are the number of nodes, m the number of edges and C the cost of the minimum cut.[39] The number of nodes n scales with the complexity of the signal model and unwrapping range needed while m also scales quadratically with the number of nodes n.[11,40] The achieved estimation times per in-phase field map in the present work was below 10 s for all cases, while water–fat separation-based field-mapping in a similar breast scan can take up to 1 h using the same graph-cut method.[13]

Second, although the selection of echo times for water–fat separation seems more flexible when compared to single-peak or *effective* multipeak in-phase echo times, this is generally not true. Echo times for water–fat separation have to be carefully selected and are itself subject to optimization. For example, the first echo time and the echo time step has to be chosen for robust species separation and high SNR,[13] and are both of the order of 1 ms at 3T. To achieve a reasonable resolution while acquiring the above echo times and using monopolar gradients, sequences such as a time-interleaved multi-echo gradient echo sequence[14] are necessary, which was presently adopted. However, the above sequence comes at the cost of increased scan time. When two shots are employed only half of the echo times are recorded per TR hence approximately doubling the scan time. In order to achieve a reasonable total scan time the maximum echo time is reduced to reduce the TR. However, a late maximum echo time can be desirable in the realm of susceptibility mapping due to the increased susceptibility weighting of the later echoes.

Finally, susceptibility mapping is well known to only estimate relative susceptibility maps, since the dipole kernel is zero at the center of $k-$space. Therefore, a reference strategy is needed to compare different dipole inversion method within one subject, and, more importantly, to allow for cross-subject comparison. In the liver, the subcutaneous fat and the paraspinal muscle were used for referencing since they are both known to not accumulate iron, which is important for the assessment of iron accumulation in the liver.[8] Referencing was also employed for the numerical liver simulation for the comparison of the different methods and was based on the subcutaneous fat. In the spine, the difference between the posterior subcutaneous fat and the CSF was measured and in the breast

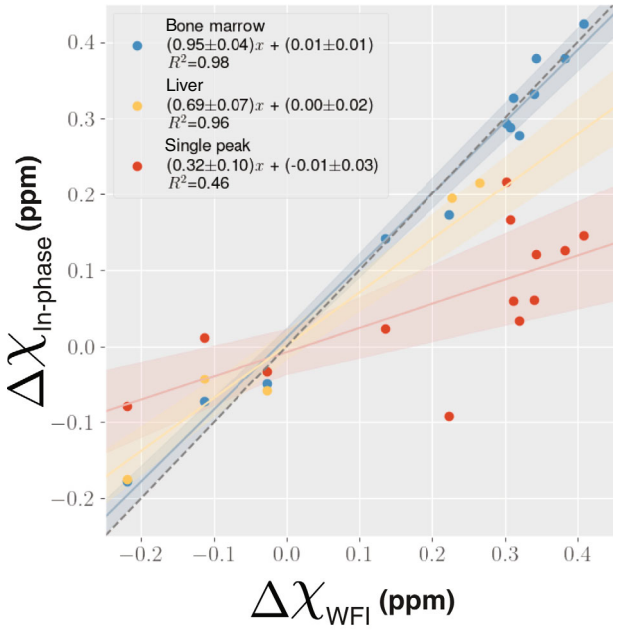

FIGURE 8 Correlation between reference water–fat separation-based susceptibility difference measurements and difference measurements based on (*effective*) in-phase acqusitions of all volunteer scans. The correlation based on single-peak in-phase echoes shows a significant underestimation of susceptibility and strong variability. Effective *in-phase* echoes based on the liver model shows a better correlation with the reference while *effective* in-phase echoes based on the bone marrow model is almost identical with the reference with the smallest variability.

the difference between fatty breast tissue and fibroglandular tissue was measured. In the spine, only the posterior subcutaneous fat was chosen since the anterior part of the body is affected by motion due to the free breathing nature of the acquisition protocol. In the brain, the CSF is often used as a reference and is assumed to have a susceptibility of zero.[34] Therefore the difference between subcutaneous fat and CSF in the spine region should be constant for different methods and even between subjects. When using *effective* multipeak in-phase echo times based on the bone marrow model, the measured susceptibility difference in all three anatomies is similar to the water–fat separation-based difference. The water–fat separation-based susceptibility maps can serve as a reference measurement for the removal of phase contributions of fat in the field map, since water–fat separation-based field maps are not prone to erroneous fat phase contributions. Particularly noteworthy is that field- and susceptibility mapping in the numerical simulation based on the bone marrow model achieved lower NRMSE in both multipeak *effective* in-phase echoes acquisition and water–fat separation when compared to the liver model. The same can be observed in the in vivo liver, where the difference measurements based on the liver fat model shows a larger deviation in reference to water–fat separation than when based on the bone marrow model. In the case of referencing in the subcutaneous fat, this can be explained by the employed referencing strategy and the different fat fractions in the liver and subcutaneous fat. The subcutaneous fat has a fat fraction of above 80% and is significantly higher than for fatty livers which can have up to 40%. In the cross-model field map quantification bias simulation with fat fraction shown in Figure 2 it was shown that the error correlates quadratically with the fat fraction. Therefore, when the relative susceptibility between subcutaneous fat and liver is tried to be measured, the error is smaller when the error in the subcutaneous fat is minimized. In the case of referencing the liver to the paraspinal muscle the improved results based on the bone marrow model may originate from the reduction of the total field map estimation error. The paraspinal muscle is close to subcutaneous fat and field map estimation error in the fat potentially propagates nonlocally into the susceptibility map.

The use of *effective* multipeak in-phase echoes still has one apparent limitation. The presently adopted liver and bone marrow signal model used for the definition of the respective *effective* multipeak in phase echoes only represent a fraction of fatty tissue compositions. In fact, most of the different adipose tissue types show a different fat composition including abdominal superficial subcutaneous adipose tissue, deep subcutaneous adipose tissue, visceral adipose tissue and the aforementioned bone marrow and liver fat compositions.[24] For all the above fat models different *effective* multipeak in-phase echo times can be defined. However, based on the tissue of interest and the employed referencing strategy, one set of *effective* multipeak in-phase echo times has to be selected. However, only the liver spectral fat model shows a significantly different composition when compared to all other fat models. In this work it was shown that field- and susceptibility-mapping based on *effective* multipeak in-phase echoes derived from the bone marrow fat model show less quantification bias then in-phase echoes based on the liver fat model. This is also true, when the liver is the tissue of interest and, more importantly, the referencing strategy is based in non-fatty regions such as the paraspinal muscle. Arguably, the in-phase echoes based on the bone marrow fat model might be the best choice for all fat-containing anatomies.

5 | CONCLUSION

The use of of *effective* multipeak in-phase echo times was proposed for QSM in water–fat regions. The proposed in-phase echoes successfully remove the field map quantification bias of single-peak based in-phase echoes and show similar results to water–fat separation based field-

and susceptibility-mapping. The use of *effective* multipeak in-phase echoes allows for a rapid field map estimation due to the simplified signal model and can reduce the scan time compared to a time interleaved multi-echo gradient echo sequence.

ACKNOWLEDGMENTS

This study was supported by the European Research Council (grant agreement no. 677661, ProFatMRI). This study only reflects the authors' view and the EU is not responsible for any use that may be made of the information it contains. The authors also acknowledge the research support provided by Philips Healthcare. The authors would like to thank Dr. Stefan Ruschke for providing the implementation of the time interleaved multi-echo gradient echo sequence. Open Access funding enabled and organized by Projekt DEAL.

CONFLICT OF INTEREST

Jakob Meineke is employee of Philips Research, Kilian Weiss is employee of Philips GmbH Market DACH, Dimitrios Karampinos receives grant support from Philips Healthcare.

ORCID

Christof Boehm https://orcid.org/0000-0003-1321-5804
Jakob Meineke https://orcid.org/0000-0001-8663-1468

TWITTER

Christof Boehm @BoehmChristof

REFERENCES

1. Wang Y, Liu T. Quantitative susceptibility mapping (QSM): decoding MRI data for a tissue magnetic biomarker. *Magn Reson Med*. 2014;73:82-101. doi:10.1002/mrm.25358
2. Boehm C, Sollmann N, Meineke J, et al. Preconditioned water-fat total field inversion: application to spine quantitative susceptibility mapping. *Magn Reson Med*. 2022;87:417-430. 10.1002/mrm.28903
3. Schweser F, Hermann KH, Deistung A, et al. Quantitative magnetic susceptibility mapping (QSM) in breast disease reveals additional information for mr-based characterization of carcinoma & calcification. Proceedings 19 Annual Meeting International Society for Magnetic Resonance in Medicine, Montreal; 2011:1014.
4. Dimov AV, Liu Z, Spincemaille P, Prince MR, Du J, Wang Y. Bone quantitative susceptibility mapping using a chemical species-specific R2* signal model with ultrashort and conventional echo data. *Magn Reson Med*. 2017;79:121-128. doi:10.1002/mrm.26648
5. Diefenbach MN, Meineke J, Ruschke S, Baum T, Gersing A, Karampinos DC. On the sensitivity of quantitative susceptibility mapping for measuring trabecular bone density. *Magnet Reson Med*. 2018;81:1739-1754. doi:10.1002/mrm.27531
6. Chen Y, Guo Y, Zhang X, Mei Y, Feng Y, Zhang X. Bone susceptibility mapping with MRI is an alternative and reliable biomarker of osteoporosis in postmenopausal women. *Eur Radiol*. 2018;28:5027-5034. doi:10.1007/s00330-018-5419-x
7. Guo Y, Chen Y, Zhang X, et al. Magnetic susceptibility and fat content in the lumbar spine of postmenopausal women with varying bone mineral density. *J Magn Reson Imaging*. 2018;49:1020-1028. doi:10.1002/jmri.26279
8. Sharma SD, Hernando D, Horng DE, Reeder SB. Quantitative susceptibility mapping in the abdomen as an imaging biomarker of hepatic iron overload. *Magn Reson Med*. 2014;74:673-683. doi:10.1002/mrm.25448
9. Lin H, Wei H, He N, et al. Quantitative susceptibility mapping in combination with water–fat separation for simultaneous liver iron and fat fraction quantification. *Eur Radiol*. 2018;28:3494-3504. doi:10.1007/s00330-017-5263-4
10. Jafari R, Sheth S, Spincemaille P, et al. Rapid automated liver quantitative susceptibility mapping. *J Magn Reson Imaging*. 2019;50:725-732. doi:10.1002/jmri.26632
11. Boehm C, Diefenbach MN, Makowski MR, Karampinos DC. Improved body quantitative susceptibility mapping by using a variable-layer single-min-cut graph-cut for field-mapping. *Magn Reson Med*. 2021;85:1697-1712. doi:10.1002/mrm.28515
12. Pineda AR, Reeder SB, Wen Z, Pelc NJ. Cramér-rao bounds for three-point decomposition of water and fat. *Magn Reson Med*. 2005;54:625-635. doi:10.1002/mrm.20623
13. Stelter JK, Boehm C, Ruschke S, et al. Hierarchical multi-resolution graph-cuts for water-fat-silicone separation in breast MRI. *IEEE Trans Med Imaging*. 2022;41:1. doi:10.1109/TMI.2022.3180302
14. Ruschke S, Eggers H, Kooijman H, et al. Correction of phase errors in quantitative water–Fat imaging using a monopolar time-interleaved multi-echo gradient echo sequence. *Magn Reson Med*. 2016;78:984-996. doi:10.1002/mrm.26485
15. Hernando D, Haldar JP, Sutton BP, Ma J, Kellman P, Liang ZP. Joint estimation of water/fat images and field inhomogeneity map. *Magn Reson Med*. 2008;59:571-580. doi:10.1002/mrm.21522
16. Lu W, Hargreaves BA. Multiresolution field map estimation using golden section search for water–fat separation. *Magn Reson Med*. 2008;60:236-244. doi:10.1002/mrm.21544
17. Yu H, Reeder SB, Shimakawa A, Brittain JH, Pelc NJ. Field map estimation with a region growing scheme for iterative 3-point water–Fat decomposition. *Magn Reson Med*. 2005;54:1032-1039. doi:10.1002/mrm.20654
18. Cui C, Shah A, Wu X, Jacob M. A rapid 3D fat-water decomposition method using globally optimal surface estimation (R-GOOSE). *Magn Reson Med*. 2017;79:2401-2407. doi:10.1002/mrm.26843
19. Cui C, Wu X, Newell JD, Jacob M. Fat water decomposition using globally optimal surface estimation (goose) algorithm. *Magn Reson Med*. 2014;73:1289-1299. doi:10.1002/mrm.25193
20. Hernando D, Kühn JP, Mensel B, et al. R2* estimation using "in-phase" echoes in the presence of fat: the effects of complex spectrum of fat. *J Magn Reson Imaging*. 2012;37:717-726. doi:10.1002/jmri.23851
21. Boehm C, Diefenbach MN, Kronthaler S, Meineke J, Weiss K, Makowski MR, Karampinos DC. Quantitative susceptibility mapping in water-fat regions using in-phase echoes introduces

significant quantification bias. Proceedings of the Annual Meeting International Society for Magnetic Resonance in Medicine; 2021:3972.
22. Yu H, Shimakawa A, McKenzie CA, Brodsky E, Brittain JH, Reeder SB. Multiecho water–Fat separation and simultaneous r2* estimation with multifrequency fat spectrum modeling. *Magn Reson Med*. 2008;60:1122-1134. doi:10.1002/mrm.21737
23. Guo Y, Liu Z, Wen Y, et al. Quantitative susceptibility mapping of the spine using in-phase echoes to initialize inhomogeneous field and R2* for the nonconvex optimization problem of fat-water separation. *NMR Biomed*. 2019;32:e4156. doi:10.1002/nbm.4156
24. Hamilton G, Schlein AN, Middleton MS, et al. In vivo triglyceride composition of abdominal adipose tissue measured by 1 H Mrs At 3T. *J Magn Reson Imaging*. 2016;45:1455-1463. doi:10.1002/jmri.25453
25. Ren J, Dimitrov I, Sherry AD, Malloy CR. Composition of adipose tissue and marrow fat in humans By1h Nmr At 7 tesla. *J Lipid Res*. 2008;49:2055-2062. doi:10.1194/jlr.d800010‐jlr200
26. Hamilton G, Yokoo T, Bydder M, et al. In vivo characterization of the liver fat 1h Mr spectrum. *NMR Biomed*. 2010;24:784-790. doi:10.1002/nbm.1622
27. Gosselin MC, Neufeld E, Moser H, et al. Development of a new generation of high-resolution anatomical models for medical device evaluation: the virtual population 3.0. *Phys Med Biol*. 2014;59:5287-5303. doi:10.1088/0031-9155/59/18/5287
28. Collins CM, Yang B, Yang QX, Smith MB. Numerical calculations of the static magnetic field in three-dimensional multi-tissue models of the human head. *Magn Reson Imaging*. 2002;20:413-424. doi:10.1016/s0730-725x(02)00507-6
29. Maril N, Collins CM, Greenman RL, Lenkinski RE. Strategies for shimming the breast. *Magn Reson Med*. 2005;54:1139-1145. doi:10.1002/mrm.20679
30. Liu Z, Kee Y, Zhou D, Wang Y, Spincemaille P. Preconditioned total field inversion (TFI) method for quantitative susceptibility mapping. *Magn Reson Med*. 2016;78:303-315. doi:10.1002/mrm.26331
31. Bydder M, Girard O, Hamilton G. Mapping the double bonds in triglycerides. *Magn Reson Imaging*. 2011;29:1041-1046.
32. Muller N, Reiter RC. Temperature dependence of chemical shifts of protons in hydrogen bonds. *J Chem Phys*. 1965;42:3265-3269. doi:10.1063/1.1696408
33. Dong J, Liu T, Chen F, et al. Simultaneous phase unwrapping and removal of chemical shift (SPURS) using graph cuts: application in quantitative susceptibility mapping. *IEEE Trans Med Imaging*. 2015;34:531-540. doi:10.1109/tmi.2014.2361764
34. Liu Z, Spincemaille P, Yao Y, Zhang Y, Wang Y. Medi+0: morphology enabled dipole inversion with automatic uniform cerebrospinal fluid zero reference for quantitative susceptibility mapping. *Magn Reson Med*. 2017;79:2795-2803. doi:10.1002/mrm.26946
35. Somasundaram A, Wu M, Borde T. Automated breast segmentation using deep-learning in water-fat breast MRI: application to breast density assessment. Proceedings of the 30th International Society for Magnetic Resonance in Medicine, London, UK; 2022:1683.
36. Tsao J, Jiang Y. Hierarchical ideal: fast, robust, and multiresolution separation of multiple chemical species from multiple echo times. *Magn Reson Med*. 2012;70:155-159. doi:10.1002/mrm.24441
37. Diefenbach MN, Liu C, Karampinos DC. Generalized parameter estimation in multi-echo gradient-echo-based chemical species separation. *Quant Imaging Med Surg*. 2020;10:554-567. doi:10.21037/qims.2020.02.07
38. Hernando D, Kellman P, Haldar JP, Liang ZP. Robust water/fat separation in the presence of large field inhomogeneities using a graph cut algorithm. *Magn Reson Med* 2009; 22177; 63:doi:10.1002/mrm.22177
39. Boykov Y, Kolmogorov V. An experimental comparison of min-cut/max- flow algorithms for energy minimization in vision. *IEEE Trans Pattern Anal Mach Intell*. 2004;26:1124-1137. doi:10.1109/tpami.2004.60
40. Shah A, Abámoff MD, Wu X. Optimal surface segmentation with convex priors in irregularly sampled space. *Med Image Anal*. 2019;54:63-75.

SUPPORTING INFORMATION

Additional supporting information may be found in the online version of the article at the publisher's website.

Figure S1. Correlation between susceptibility and field map based on a forward simulation at a sphere and an infinite surface. The correlation for a spherical surface and an infinite surface is −0.304 and −0.332 when the surface is parallel to B_0 and 0.608 and 0.664 when the surface is perpendicular to B_0, respectively. Based on the results in Figure 2, the field map quantification bias in a voxel with a fat fraction of 100% measured with single-peak in phase echo translates into a susceptibility estimation error of $\frac{-0.1\text{ppm}}{-0.304} = 0.33$ ppm in the liver and $\frac{-0.13\text{ppm}}{-0.304} = 0.43$ ppm in bone marrow, respectively.

Table S1: Mean susceptibility, standard deviation and size of all ROIs for all scans. In brackets the region of the ROI is given (fat, muscle, fibroglandular, etc.). The subscripted text refers to the estimation method, hence $\overline{\chi}(\text{fibroglandular})_{\text{WFI}}$ refers to the mean susceptibility and standard deviation of fibroglandular tissue based on waterŰfat separation field map estimation.

How to cite this article: Boehm C, Schlaeger S, Meineke J, Weiss K, Makowski MR, Karampinos DC. On the water–fat in-phase assumption for quantitative susceptibility mapping. *Magn Reson Med*. 2023;89:1068-1082. doi: 10.1002/mrm.29516